Hindawi Publishing Corporation
Journal of Materials
Volume 2013, Article ID 802123, 10 pages
http://dx.doi.org/10.1155/2013/802123

*Research Article*

# Conduction Mechanism by Using CBH Model in $Fe^{3+}$ and $Mn^{3+}$ Ion Modified $Pb(Zr_{0.65-x}A_xTi_{0.35})O_3$ (A = $Mn^{3+}$/$Fe^{3+}$) Ceramics

**Niranjan Sahu,[1] S. Panigrahi,[2] and Manoranjan Kar[3]**

[1] *Department of Physics, Purushottam Institute of Engineering and Technology, Rourkela, Odisha 770034, India*
[2] *Department of Physics, National Institute of Technology, Rourkela, Odisha 769008, India*
[3] *Department of Physics, Indian Institute of Technology, Patna, Bihar, 800013, India*

Correspondence should be addressed to Niranjan Sahu; drniranjannitr@gmail.com

Received 14 December 2012; Accepted 21 January 2013

Academic Editor: Iwan Kityk



Polycrystalline samples of manganese and iron substituted lead zirconium titanate (PZT) with general formula $Pb(Zr_{0.65-x}A_xTi_{0.35})O_3$ (A = $Mn^{3+}$ and $Fe^{3+}$) ceramics have been synthesized by high temperature solid state reaction technique. X-ray diffraction (XRD) patterns were recorded at room temperature to study the crystal structure. All the patterns could be refined by employing the Rietveld method to *R3c* space group with rhombohedral symmetry. Microstructural properties of the materials were analyzed by scanning electron microscope (SEM), and compositional analysis was carried out by energy dispersive spectrum (EDS) measurements. All the materials exhibit ferroelectric to paraelectric transition. The variation of dielectric constant and loss tangent with temperature and frequency is investigated. The decrease of activation energy and increases of AC conductivity with the $Fe^{3+}$ or $Mn^{3+}$ ion concentration have been observed. The AC conductivity has been analyzed by the power law. The frequency exponent with the function of temperature has been analyzed by assuming that the AC conduction mechanism is the correlated barrier hopping (CBH) model. The conduction in the present sample is found to be of bipolaron type for $Mn^{3+}$ ion-doped sample. However, the conduction mechanism could not be explained by CBH model for $Fe^{3+}$ ion-doped sample.

## 1. Introduction

Pb-based ceramic oxides have been widely studied due to their excellent ferroelectric, dielectric, and piezoelectric properties [1–3]. In particular, $PbTiO_3$-based solid solutions have dominated for decades the technological field responsible for the development of piezoelectric materials [4]. Lead zirconium titanate (PZT) belongs to the perovskite structural family of a general formula $ABO_3$ in which A site is occupied by $Pb^{2+}$ ions and B site by $Zr^{4+}$ or/and $Ti^{4+}$ ions [1–3]. Fluctuation of the oxidation state of $Mn^{3+}$/$Fe^{3+}$ ions results in the formation of oxygen ion vacancies to reserve the local electrical neutrality and causes thermally activated conduction. PZT is a solid solution of ferroelectric $PbTiO_3$ (PT with $T_c$ = 490°C) and antiferroelectric $PbZrO_3$ (PZ with $T_c$ = 230°C) with different Zr/Ti ratios and has two ferroelectric phases: a tetragonal phase in the titanium rich side of the binary system and a rhombohedral phase in the zirconium rich side [5, 6]. The boundary line between these two phases is called morphotropic phase boundary (MPB) at which dielectric and conductive properties rise to a great extent [7]. A wide variety of complex compounds (other than the above) can be prepared by substituting suitable elements at the A and B sites of PZT useful for different industrial applications such as dynamic and versatile memory components, capacitors, transducers, sensors, and light liquid crystal display backlight inverters for camcorder [8–10]. The selection of substituents to tailor the physical properties of the material is based on many factors including charge neutrality, tolerance factor, the ionic radius, and solubility. Magnetic materials (Mn and Fe) have been widely used as a doping element for the manufacturing of multilayer ceramic capacitor. Mn and Fe doping in PZT causes the lowering of the Curie temperature and grain size [11].

Recently, Tiwari and Choudhary [12] showed that the substitution of Mn and Ce on Zr site leads to an improvement of dielectric constant and shift in $T_c$. Sahu et al. [13] observed that substitution of Mn (in small amounts) at the Zr site of

PZT does not provide any change in its structure. Mn doping changes the particle density on the surface.The detailed literature survey reveals that not much work has been done on low doping of both Mn and Fe modified PZT ceramics [14–16]. However, dielectric and AC conductivity studies of both the ion modified PZT and related materials have hardly been reported in the literature [17–20]. The ratio of Zr/Ti (65/35) forms a part of our study, which includes ratios in and around MPB [21, 22]. Keeping in view these facts, we have carried out detailed studies of the Rietveld structural and microparameter analysis and microstructure, dielectric, and AC conductivity studies of $Mn^{3+}$ and $Fe^{3+}$ ions modified from PZT (Zr/Ti = 65/35) prepared by conventional solid state reaction route. In this paper, the Rietveld analysis is used to refine structure and microparameter of Mn and Fe substitution on B site of PZT material.

Structural studies of this materials are very important for a better understanding of transport mechanisms. AC conductivity measurements have been widely used to investigate the nature of defect centers in disordered systems since it is assumed that they are responsible for this type of conduction. The general frequency behavior in this type of materials is of $A\omega^n$ type over a wide frequency range where exponent s is found to be temperature dependent and has a value $\leq 1$. The correlated barrier-hopping (CBH) model [23] has been extensively applied to semiconducting materials. According to this model, the conduction occurs via bipolaron hopping process wherein two electrons simultaneously hop over the potential barrier between two charged defect states ($D^+$ and $D^-$) and the barrier height is correlated with the inter site separation via a Coulombic interaction. Shimakawa and Itoh [24] suggested further that, at higher temperatures, $D_o$ states are produced by thermal excitation of $D^+$ and $D^-$ states and single polaron hopping (i.e., one electron hopping between $D^o$ and $D^+$ and a hole between $D^o$ and $D^-$) becomes a dominant process. The concept of the CBH model, incorporating the suggestions of Shimakawa and Itoh, is applied to the present data. Here the main goal of this paper is to strongly discuss the structural analysis of the Rietveld refinement technique has strongly discussed with few dielectric analysis. The novelty of this paper is what the conduction mechanism explains about the type of bipolaron materials.

## 2. Experimental

Perovskite $Pb(Zr_{0.65-x}A_xTi_{0.35})O_3$ (A = Mn and Fe, $x = 0.0, 0.05$) ceramic has been prepared by solid state method. Stoichiometric ratio of PbO (Loba Chemie, Mumbai, India), $ZrO_2$ (Loba Chemie, Mumbai, India), $MnO_2$ (E. Merck India Ltd.), $Fe_2O_3$ (E. Merck India Ltd.), and $TiO_2$ (E. Merck India Ltd.) with 99.9% purity was weighed by using a high precision electronic balance (Avon, Gr 202). The above materials were mixed thoroughly with the help of Agate mortar and pestle. The grinding was carried out under acetone till the acetone evaporates from the mortar. The mixture was ball milled for 8 hrs and presintered at different temperatures with intermediate grindings. The final presintered temperature was 900°C for 4 hrs. The calcined powders of the above compounds were pressed into cylindrical pellets of 6 mm diameter and 1 mm thickness under a uniaxial pressure of 6 tons using a hydraulic press. Polyvinyl alcohol (PVA) was used as the binder to prepare the pellets. Finally, the pellets were sintered at 1100°C for over 4 hrs in an alumina crucible. The density of the electronic ceramic is a very sensitive parameter that directly affects its properties. Therefore, proper sintering of the pellets is essential for electrical measurement. All the pellets were taken on an alumina plate and sintered at different temperatures in a programmable furnace. A lead rich atmosphere was maintained to minimize lead loss during sintering. All the above sintering processes were carried out in air. XRD pattern at room temperature for the sample was recorded by using Philips PANalytical X'Pert-MPD X-ray diffractometer (XRD) (model: PW3020). The CuK$\alpha$ radiation was used as an X-Ray source. The machine was operated at 35 KV and 30 mA in a wide range of Bragg angles $2\theta$ ($20^\circ \leq 2\theta \leq 80^\circ$). The data were collected with step size of 0.020 and time constant of 1 second. The scanning electron micrograph was recorded using JEOL SEM (JEOL T-330) at room temperature. The compositional analysis was carried out by SEM-EDS. The pellets are made with high-purity silver paint electrodes on the flat polished surfaces and heated at 150°C for 2 hrs to take dielectric and electrical measurements. The dielectric (capacitance and dissipation) and impedance parameters (phase angle) were obtained at an Ac input signal level of 1.5 V in a wide temperature (40–500°C) and frequency (100 Hz–625 kHz) ranges using a computer-controlled LCR HiTESTER/Impedance analyzer (HIOKI 3522-50) which is also attached with high temperature microwave furnace (model: DPI-1200).

## 3. Results and Discussion

*3.1. Structural Analysis by Employing the Rietveld Method.* Figure 1 shows the X-ray diffraction pattern of powders calcined at temperature 900°C for 4 hrs of Pb $(Zr_{0.65-x}A_xTi_{0.35})O_3$ (A = Mn, Fe) ($x = 0.0, 0.05$). All the samples are in single-phase form. Figure 2 shows the XRD pattern of the samples sintered at 1100°C for 4 hrs. XRD peaks for 1100°C annealed samples are sharper compared to those of 900°C annealed samples which reveals that the crystallite size increases with the temperature (discussed in the next section). The patterns clearly indicate that there is no structural change of $Pb(Zr_{0.65-x}A_xTi_{0.35})O_3$ (A = Mn, Fe) ($x = 0.00, 0.05$) on substitution of small amount of $Mn^{3+}/Fe^{3+}$ ion at the Zr site. It is observed that the structure has perovskite phase without any secondary phase, indicating the complete diffusion of $Mn^{3+}/Fe^{3+}$ ion into PZT lattice to form a single-phase compound. The unit cell parameters of rhombohedral system (space group *R3c*) were refined using the Rietveld refinement technique with the help of FullProf program, and bond lengths and bond angles were calculated with the help of powder cell program. We have obtained the average crystallite size by using the Rietveld method. A complete expression is used in the Rietveld method which is defined as [25]

$$\mathrm{FWHM}^2 = \left(U + D_{\mathrm{ST}}^2\right)\left(\tan^2\theta\right) + V\left(\tan\theta\right) + W + \frac{IG}{\cos^2\theta}, \quad (1)$$

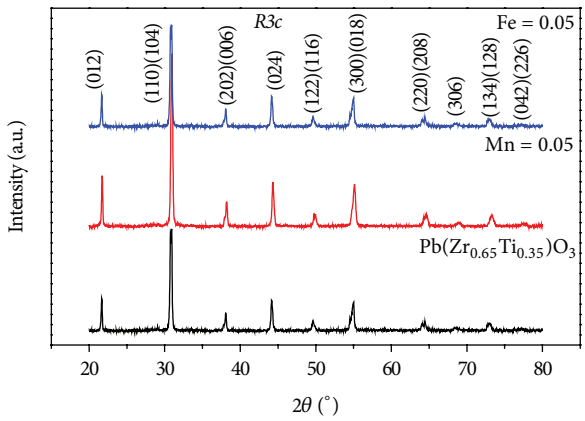


FIGURE 1: XRD patterns of the samples $Pb(Zr_{0.65}Ti_{0.35})O_3$, $Pb(Zr_{0.60}Mn_{0.05}Ti_{0.35})O_3$, and $Pb(Zr_{0.60}Fe_{0.05}Ti_{0.35})O_3$ annealed at 900°C for over 4 hrs.

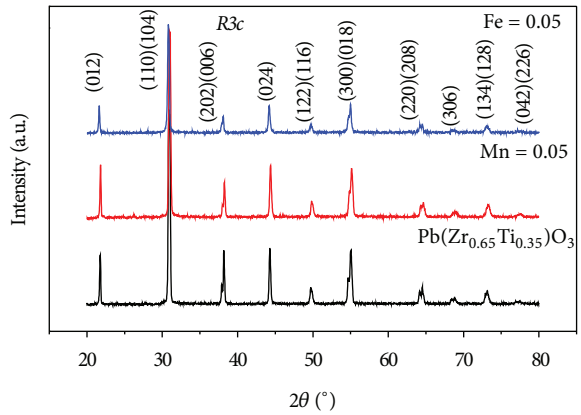


FIGURE 2: XRD Patterns of the samples $Pb(Zr_{0.65}Ti_{0.35})O_3$, $Pb(Zr_{0.60}Mn_{0.05}Ti_{0.35})O_3$, and $Pb(Zr_{0.60}Fe_{0.05}Ti_{0.35})O_3$ annealed at 1100°C for over 4 hrs.

where $U$, $V$, and $W$ are the usual peak shape parameters.The width of the diffraction peaks is found to broaden at higher Bragg angles, where $U$, $V$, and $W$ are the half width parameters and may be refined during the fit.

The estimation of crystallite size of powder samples in view of the ability of the former approach to measure the pure breadth of the diffraction peaks that is, solely due to smaller crystallite size.

$IG$ is a measure of the isotropic size effect, and $D_{ST}$ = coefficient related to strain. $IG$ and $D_{ST}$ can be refined by Rietveld method. Finally, the FWHM is used in the Scherrer's formulae to calculate the crystallite size. Scherrer's formulae are defined as [26]

$$S_C = \frac{\kappa\lambda}{\beta\cos\theta}, \quad (2)$$

where, constant "$\kappa$" depends on the shape of the crystallite size (=0.89, assuming the circular grain), $\beta$ = full width at half maximum (FWHM) of intensity versus $2\theta$ profile, $\lambda$ is the wavelength of the $CuK_\alpha$ radiation (=0.15418 nm), and $\theta$

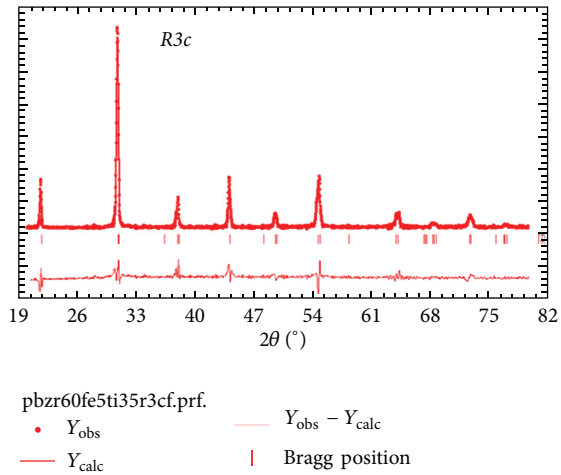


FIGURE 3: XRD pattern along with the Rietveld refined data for the sample $Pb(Zr_{0.60}Fe_{0.05}Ti_{0.35})O_3$ annealed at 1100°C for over 4 h. The data have been refined using *R3c* space group with rhombohedral symmetry.

is Bragg's diffraction angle. The average crystallite values are listed in Table 1 for both 900°C and 1100°C annealed samples. One can notice that average crystallite size increases with annealing temperature. It is due to the formation of larger crystals at high temperature, smaller ionic size, fractional atomic positions and isothermal parameters, lattice parameters, cell volume, the goodness of the fitting parameter, and so forth.

Typical refined XRD pattern $Pb(Zr_{0.60}Fe_{0.05}Ti_{0.35})O_3$ annealed at 1100°C for 4 hrs is shown in Figure 3. The experimental points are given as dot (•) and theoretical data are shown as solid line. Difference between theoretical and experimental data is shown as bottom line. The vertical line represents Bragg's allowed peak. One can notice that all the observed peaks could be well refined to *R3c* space group in rhombohedral symmetry. The lattice parameters and goodness of the fitting are listed in Table 2. Lattice parameters, occupancy, fractional atomic positions, and so forth were taken as the free parameter during the fitting. The thermal effect and profile functions refinement are fitted better than the other refinement. The pseudo-Voigt description of profile shape was determined as a profile setup for Rietveld refinement. Refinement profile function value is used for modern commercial Bragg-Brentano diffractometer and the value of the sample broadening. The lattice parameters and unit cell volumes are decreased with the doping of Mn/Fe, and it could be due to the smaller ionic size of $Mn^{3+}$ (0.66 Å)/$Fe^{3+}$(0.64 Å) compared to that of $Zr^{4+}$ (0.79 Å). Bond lengths and bond angles were calculated from the refined parameters and those values are listed in Table 2 for all the samples at 1100°C temperatures.

*3.2. Microstructural and Elemental Analysis.* The scanning electron microscopy (SEM) of pure PZT and 5% Mn and 5% Fe substitution at Zr site of the compounds are shown in Figures 4(a)–4(c), respectively. From these micrographs, it

Table 1: Crystallite size and grain size of the samples $PbZr_{0.65}Ti_{0.35}O_3$, $Pb(Zr_{0.60}Fe_{0.05}Ti_{0.35})O_3$, and $Pb(Zr_{0.60}Mn_{0.05}Ti_{0.35})O_3$ annealed at different temperatures.

| Sample composition | Crystallite size (nm) | Grain size ($\mu$m), SEM |
|---|---|---|
| $Pb(Zr_{0.65}Ti_{0.35})O_3$ (900°C) | 13.5(8) | 0.114(5) |
| $Pb(Zr_{0.65}Ti_{0.35})O_3$ (1100°C) | 33.0(1) | 3.513(6) |
| $Pb(Zr_{0.60}Fe_{0.05}Ti_{0.35})O_3$ (900°C) | 13.0(3) | 0.111(7) |
| $Pb(Zr_{0.60}Fe_{0.05}Ti_{0.35})O_3$ (1100°C) | 32.1(9) | 3.423(5) |
| $Pb(Zr_{0.60}Mn_{0.05}Ti_{0.35})O_3$ (900°C) | 12.5(4) | 0.110(9) |
| $Pb(Zr_{0.60}Mn_{0.05}Ti_{0.35})O_3$ (1100°C) | 30.1(1) | 3.323(5) |

was confirmed that the grains of different sizes are uniformly and densely distributed over the entire surface of the samples. The 5% Mn and 5% Fe doping grain size shows a decreasing trend with an increase in Mn and Fe concentration. Similar results have been observed by other groups [27].

Figures 5(a)–5(c) shows the energy dispersive X-ray spectroscopy (EDS) for all the samples. The compositions present in the sample are as prepared. Generally, Pb evaporates during the high temperature annealing. However, we have added 5% extra PbO during sintering which is already reported in this type of materials. Atomic percentage of the sample $Pb(Zr_{0.65-x}A_xTi_{0.35})O_3$ (A = Mn/Fe, $x = 0.0, 0.05$) (annealed at 1100°C) obtained from SEM-EDS is given in Table 3.

*3.3. Dielectric Analysis.* Figure 6(a) shows the variation of dielectric constant versus temperature of pure and Mn(5%)/Fe(5%) substitutions in Zr site of the compound at the frequency 10 kHz. It indicates that dielectric constant increases gradually with an increase in temperature for pure and doped samples to its maximum value and then decreases, which confirms that a phase transition (from ferroelectric to paraelectric phase) occurs at a particular temperature, called as transition or the Curie temperature ($T_c$) [27]. On further increase in temperature, the relative dielectric constant decreases for pure and substituted samples of the compound. The comparative dielectric data of pure and substituted samples at frequency 10 kHz are recapitulated in Table 4. The $T_c$ is maximum at pure sample and minimum for Mn substitution at Zr site of the compound. But one can observe that for pure PZT, the value of dielectric constant is less and $T_c$ is more. For Mn doping, dielectric constant is more but $T_c$ is less in comparison with Fe substitutions.

Plots of frequency versus dielectric constants are shown in Figure 6(b). Dielectric constant decreases with an increase of frequency for pure and substituted samples at higher temperature (500°C). It is due to the presence of all types of polarizations (i.e., interfacial, ionic, dipolar, electronic, and space charge) [28, 29]. At higher frequencies, the main contribution to dielectric constant comes from electronic polarization, as some of the polarizations become ineffective and, thus, the value of dielectric constant decreases.

*3.4. Spectral Dependence of AC Conductivity.* The AC conductivity ($\sigma_{ac}$) of the above ceramic materials can be calculated by using the relation [30]

$$\sigma_{ac} = \omega \varepsilon_o \varepsilon_r \tan \delta, \tag{3}$$

where $2\pi f = \omega$, $\varepsilon_o$ is the permittivity of free space, $\varepsilon_r$ is the relative dielectric constant, and $\tan \delta$ is the dissipation factor. The AC conductivity pattern indicates a progressive rise in conductivity with a rise in temperature at frequency 10 kHz.

Ac conductivity ($\sigma_{ac}(\omega)$) can be written as [31]

$$\sigma_{ac}(\omega) = \sigma_t(\omega) - \sigma_{dc}, \tag{4}$$

where $\sigma_t(\omega)$ is the total conductivity and $\sigma_{dc}$ is the DC conductivity. However, the $\sigma_{dc}$ is negligible compared to that of $\sigma_t(\omega)$. The AC conductivity $\sigma_{ac}(\omega)$ is given by the relation

$$\sigma_{ac}(\omega) = A\omega^n, \tag{5}$$

where $A$ is a constant, $\omega$ is the angular frequency ($\omega = 2\pi f$), and $n$ is the frequency exponent. We have obtained the value of $n$ which is less than 1. Typical plot of $\ln(\omega)$ versus $\ln(\sigma_{ac}(\omega))$ is shown in Figure 7 for the sample $Pb(Zr_{0.60}Mn_{0.05}Ti_{0.35})O_3$ at selected temperatures. The fitting has been carried out from 9 kHz to 625 kHz. Temperature versus $n$ is shown in Figure 7 for the sample $Pb(Zr_{0.60}Mn_{0.05}Ti_{0.35})O_3$. The observed behavior of $n(T)$ can be analyzed by assuming that the AC conduction mechanism is the correlated barrier hopping (CBH) model [32]. According to this model, the conduction occurs via bipolaron hopping process. Bipolaron theory suggests that two polarons simultaneously hop over the potential barrier between two charged defect states $D^+$ and $D^-$ and that the barrier height is correlated with the intersite separation via coulombic interaction. At higher temperature, $D^0$ state is produced by thermal excitation of $D^+$ and $D^-$ states and a single-polaron hopping becomes the dominant process in which there is one electron hopping between $D^0$ and $D^+$ and hole between $D^0$ and $D^-$. The frequency exponent $n(T)$ can be written as

$$n(T) = \frac{d(\ln \sigma_{ac})}{d(\ln \omega)} = 1 - \frac{6k_BT}{W_m}. \tag{6}$$

Or, one can write,

$$\beta = 1 - n(t) = \frac{6k_BT}{W_m}, \tag{7}$$

where $k_B$ is the Boltzmann constant, and $W_m$ is the maximum barrier height which is the energy required to take two electrons from the $D^-$ state to the conduction band in the absence of $D^+$ centers. Plot of $\beta$ versus $T$ is shown in Figure 8. One can see that it is a straight line. From linear fit, we have obtained $W_m$ and, it is found to be 3.34 eV. The variation of AC conductivity with frequency at different temperatures is shown in Figure 9 of the sample $Pb(Zr_{0.65-x}Fe_xTi_{0.35})O_3$.

Table 2: Parameters obtained from XRD analysis by employing the Rietveld method of $Pb(Zr_{0.65}Ti_{0.35})O_3$, $Pb(Zr_{0.60}Mn_{0.05}Ti_{0.35})O_3$, and $Pb(Zr_{0.60}Fe_{0.05}Ti_{0.35})O_3$ samples annealed at 1100°C for 4 hrs.

| Parameters | Sample | | |
|---|---|---|---|
| | $Pb(Zr_{0.65}Ti_{0.35})O_3$ | Mn = 0.05 | Fe = 0.05 |
| Space group | *R3c* | *R3c* | *R3c* |
| Pb (occupancy) | 0.9823(24) | 0.9873(8) | 0.97365(5) |
| Zr (occupancy) | 0.6451(15) | 0.6012(9) | 0.60135(7) |
| Ti (occupancy) | 0.3451(15) | 0.3476(9) | 0.3500(5) |
| $a = b$ (Å) | 5.8169(7) | 5.7863(12) | 5.8089(5) |
| $c$ (Å) | 14.18(21) | 14.17(32) | 14.15(7) |
| Volume (Å$^3$) | 415.65(10) | 413.89(15) | 413.55(9) |
| $\chi^2$ (chi$^2$) | 1.91 | 2.99 | 1.15 |
| $R_p$ | 6.9 | 6.1 | 8.2 |
| $R_{wp}$ | 10.5 | 12.1 | 13.3 |
| $R_{Bragg}$ | 6.8 | 5.7 | 5.7 |
| $R_f$ | 10.4 | 10.9 | 9.3 |
| Pb-Ti/Zr (Å) | 3.4901(2) | 3.3463(11) | 3.2731(6) |
| Ti/Zr-$O_1$ (Å) | 2.1111(2)/1.9996(11) | 2.2213(24) | 1.9983(7)/1.7382(9) |
| Ti/Zr-$O_2$ (Å) | 2.8888(10) | 3.2784(4) | 3.2731(5)/1.5891(7) |
| ∠Pb-Ti/Zr-Pb | 112.88(13) | 38.5(2) | 110.32(2) |
| ∠Pb-Ti/Zr-$O_1$ | 124.51(21) | 126.10(9) | 120.87(7) |
| ∠Pb-Ti/Zr-$O_2$ | 137.92(6) | 114.32(5) | 106.54(5) |
| ∠Mn-Pb-Mn | — | 32.25(5) | — |
| ∠Fe-Pb-Fe | — | — | 38.39(9) |
| ∠Zr-$O_2$-Zr | 95.32(5) | 92.36(6) | 101.35(2) |

Table 3: Atomic percentage of the sample $Pb(Zr_{0.65-x}A_xTi_{0.35})O_3$ (A = Mn/Fe, $x$ = 0.0, 0.05) (annealed at 1100°C) obtained from SEM-EDS.

| Composition | O wt% (atomic%) | Zr wt% (atomic%) | Mn/Fe wt% (atomic%) | Ti wt% (atomic%) | Pb (atomic%) |
|---|---|---|---|---|---|
| $x$ = 0.0 | 14.94 | 18.71 | 0.00 | 5.44 | 60.91 |
| | (60.38) | (13.26) | (0.00) | (7.35) | (19.01) |
| Mn = 0.05 | 15.56 | 17.18 | 0.21 | 5.33 | 61.72 |
| | (61.79) | (11.97) | (0.24) | (7.07) | (18.93) |
| Fe = 0.05 | 15.85 | 18.32 | 0.21 | 5.32 | 61.65 |
| | (61.83) | (12.23) | (0.24) | (7.21) | (18.35) |

Table 4: Dielectric behaviors of pure and substituted samples (Mn and Fe) at 10 kHz.

| Sample | $\varepsilon_{max}$ | $T_c$ (°C) |
|---|---|---|
| $Pb(Zr_{0.65}Ti_{0.35})O_3$ | 3549 | 363 |
| $Pb(Zr_{0.60}Mn_{0.05}Ti_{0.35})O_3$ | 14245 | 292 |
| $Pb(Zr_{0.60}Fe_{0.05}Ti_{0.35})O_3$ | 5432 | 346 |

We have not observed linearity in the curve. So the above analysis is not able to be applied for Fe-doped sample. Hence it is concluded that the AC conduction for Mn-doped sample can be explained by CBH model; however, it is not applicable for Fe-doped sample. However, we have observed that, conductivity in both Mn- and Fe-doped samples is more than that in the PZT ($PbZr_{0.65}Ti_{0.35}O_3$) sample. The conductivity of Mn doped PZT is more than that of Fe-doped PZT sample. For example, AC conductivity of samples is $1.55 \times 10^{-8}$, $0.09 \times 10^{-9}$, and $2.15 \times 10^{-10}$ S/cm for the samples $PbZr_{0.60}Mn_{0.05}Ti_{0.35}O_3$, $PbZr_{0.60}Fe_{0.05}Ti_{0.35}O_3$, and $PbZr_{0.65}Ti_{0.35}O_3$, respectively, at room temperature at 1000 Hz.

A relation between AC conductivity and temperature is defined as [33]

$$\sigma = \sigma_0 \exp\left(\frac{-E_a}{K_B T}\right), \tag{8}$$

where $\sigma_o$ is a constant, $K_B$ is the Boltzmann constant, and $E_a$ is the activation energy for conduction. The activation energy decreases from Mn to Fe substitution in the low temperature region (ferroelectric region). All the activation energies are recapitulated in Table 5 with different temperature ranges. We have observed that activation energy in

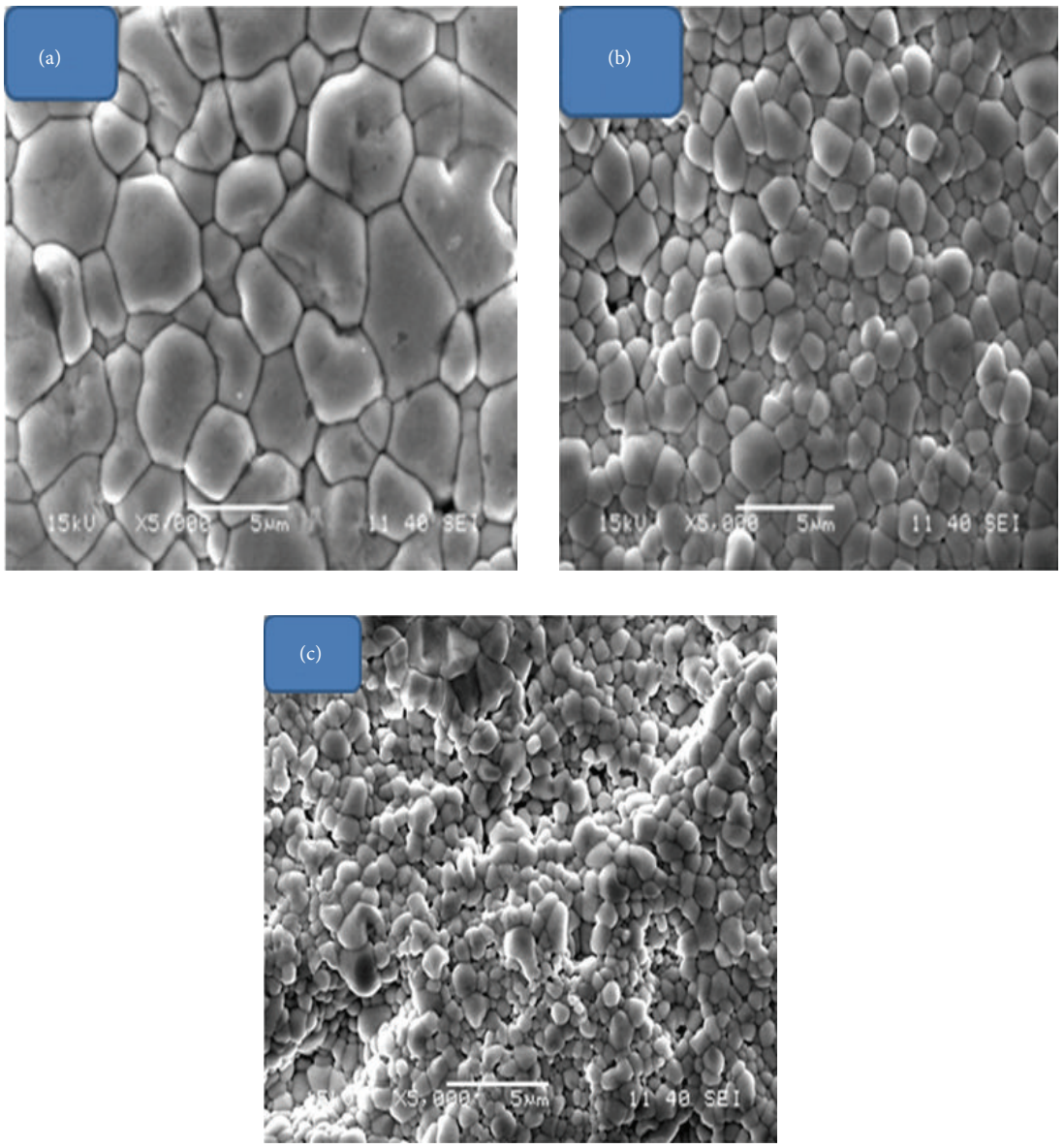


Figure 4: (a–c) SEM micrographs of the sample $PbZr_{0.65}Ti_{0.35}O_3$, $Pb(Zr_{0.60}Mn_{0.05}Ti_{0.35})O_3$ and $Pb(Zr_{0.60}Fe_{0.05}Ti_{0.35})O_3$ annealed at 1100°C for 4 hrs.

both Mn- and Fe-doped samples is less than that of the PZT ($PbZr_{0.65}Ti_{0.35}O_3$) sample. The activation energy of Mn-doped PZT is less than that of Fe-doped PZT sample. The activation energy is found to be maximum at ferroelectric region and minimum at paraelectric region for both the samples (Mn- and Fe-doped PZT). This is due to the ionic size and tolerance factor of the materials. The type of temperature dependent of AC conductivity indicates that the electrical conduction in the material is a thermally activated process. It is well known that the motion of oxygen vacancies gives rise to activation energy of 1 eV in ceramic samples; usually oxygen vacancies are considered as one of the mobile charge carriers in perovskites ferroelectric [34]. The ionization of oxygen vacancies creates conducting electrons, which are easily thermally activated. From the results of conduction and the value of the activation energy for conduction, clearly suggests a possibility that the conduction in the higher temperature range for charge carriers may be due to oxygen vacancies and some other several factors like ions, electrons, electron-phonon modes, thermal local expansions, and so forth [35]. The variation of AC conductivity of the sample $Pb(Zr_{0.65-x}Fe_xTi_{0.35})O_3$ ($x = 0.05$) with frequency at different temperatures is shown in Figures 10(a)–10(c).

## 4. Conclusions

The Mn/Fe modified PZT ($PbZr_{0.65}Ti_{0.35}O_3$) has been prepared in a single-phase form. The XRD patterns could be refined by employing the Rietveld refinement technique to

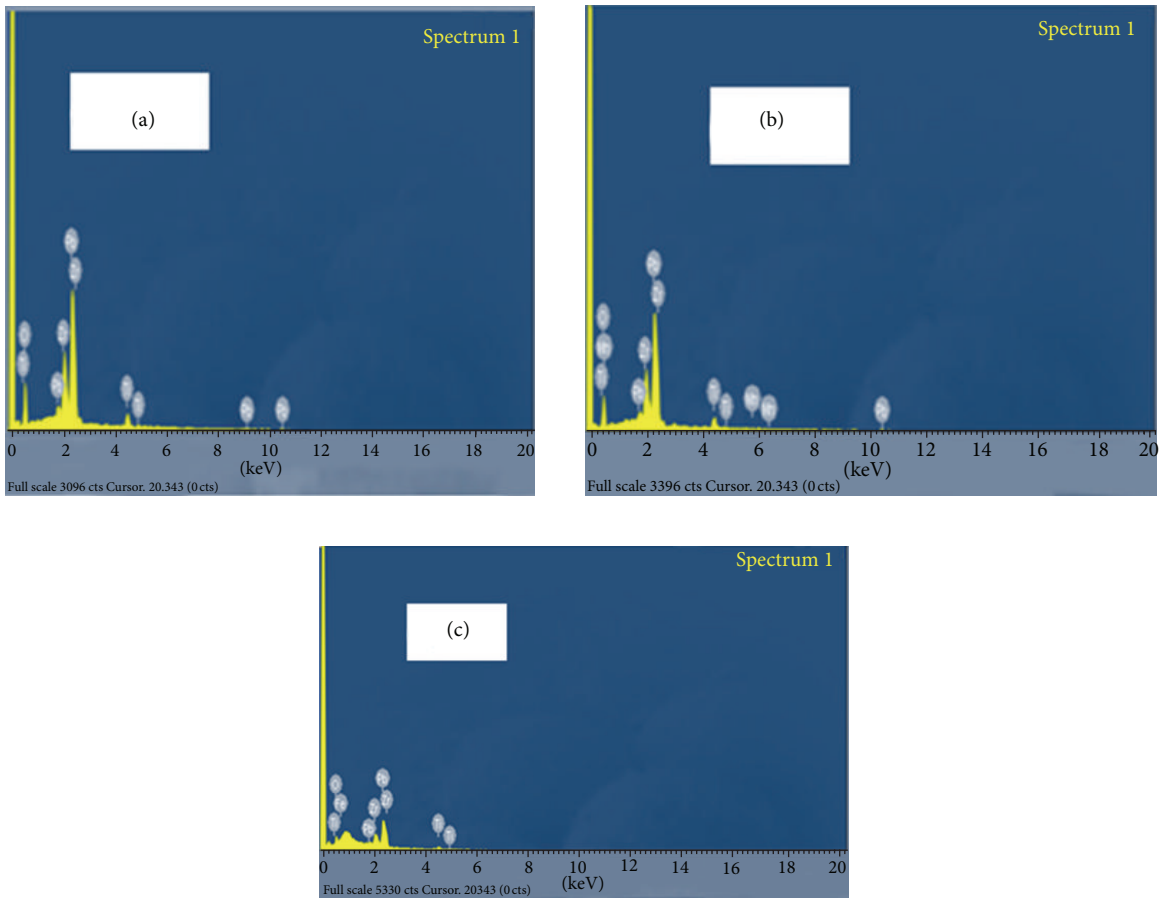


FIGURE 5: (a–c) EDS of $Pb(Zr_{0.65-x}A_xTi_{0.35})O_3$ (A = Mn/Fe) for (a) $x = 0.0$, (b) Mn = 0.05 and (c) Fe = 0.05 samples sintered at 1100°C for 4 hrs.

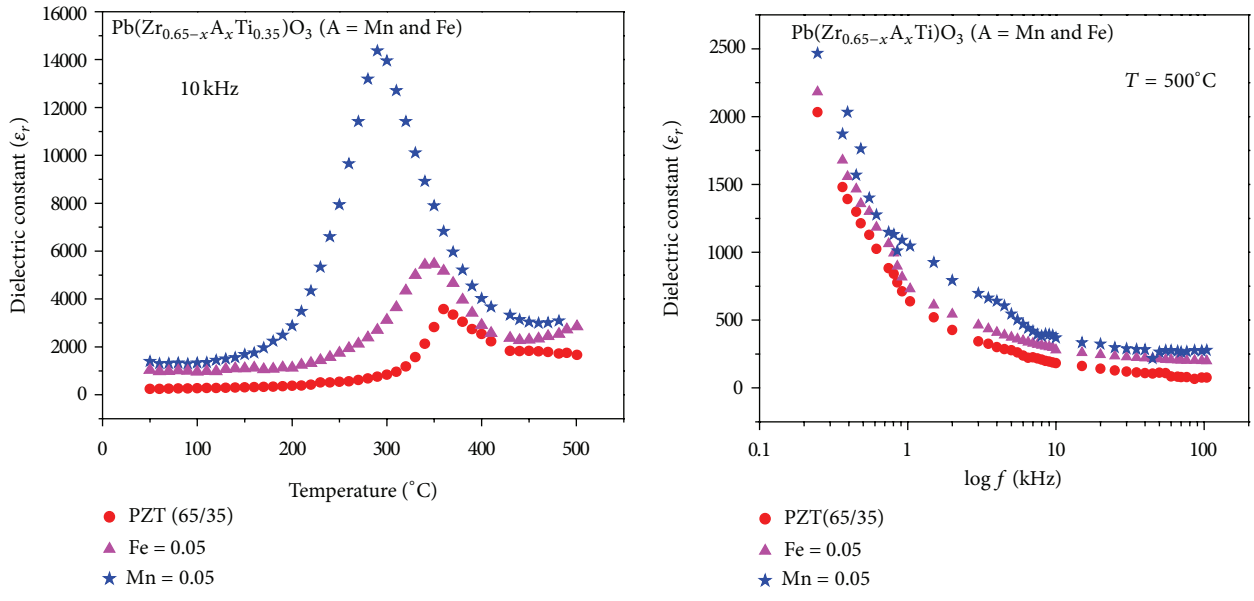


FIGURE 6: (a) shows the variation of dielectric constant with temperature at frequency 10 kHz and (b) shows the variation of dielectric constant with log$f$ at 500°C temperature for the samples $PbZr_{0.65}Ti_{0.35}O_3$, $Pb(Zr_{0.60}Mn_{0.05}Ti_{0.35})O_3$, and $Pb(Zr_{0.60}Fe_{0.05}Ti_{0.35})O_3$, respectively.

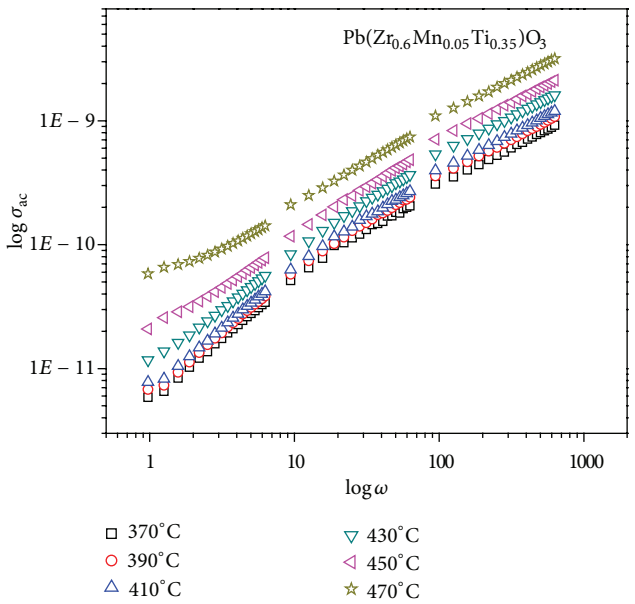


FIGURE 7: ln ($\omega$) versus ln($\sigma_{ac}(\omega)$) for the sample $Pb(Zr_{0.60}Mn_{0.05}Ti_{0.35})O_3$ at selected temperatures.

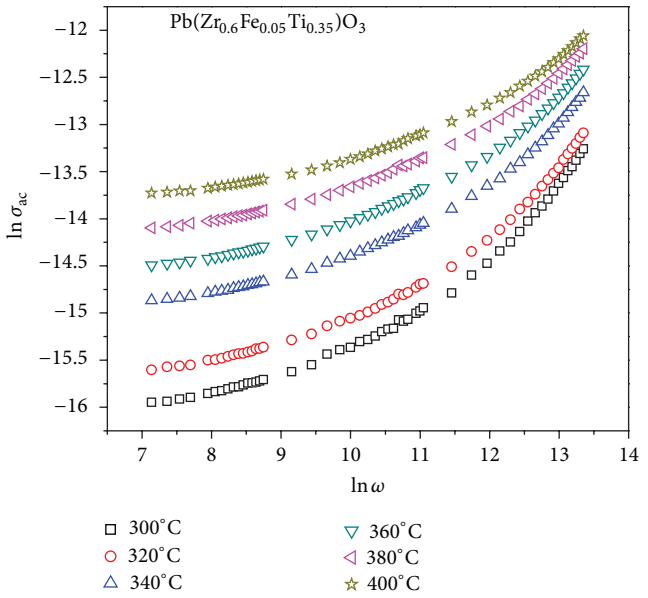


FIGURE 9: Variation of AC conductivity of the sample $Pb(Zr_{0.65-x}Fe_xTi_{0.35})O_3$ ($x = 0.05$) with frequency at different temperatures with error bar being plus or minus 1.5%.

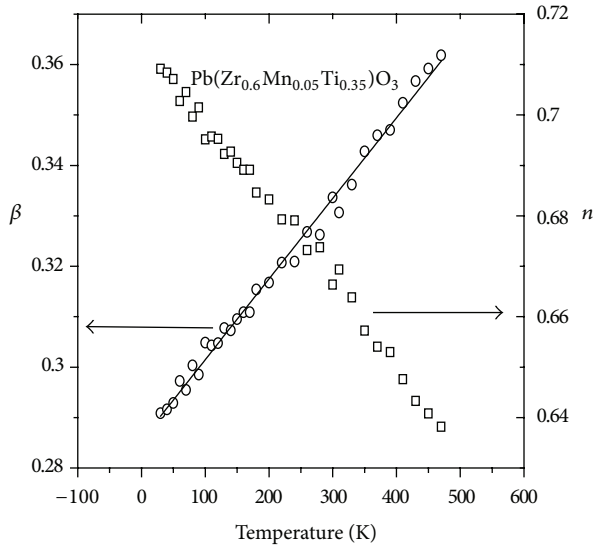


FIGURE 8: Plots of $n(T)$ of $\beta(T)$ versus temperature ($T$) for the sample $Pb(Zr_{0.60}Mn_{0.05}Ti_{0.35})O_3$. Solid line shows the linear fit.

TABLE 5: Activation energies of the $Pb(Zr_{0.65-x}A_xTi_{0.35})O_3$ (A = Mn and Fe) at $x = 0.05$ sample in below and above transition temperature range at frequency 10 kHz in relation with AC conductivity plots, Figures 7(a)–7(c).

| Temperature range (°C) | Frequency (kHz) | Activation energy (eV) |
|---|---|---|
| 180–280 (Mn = 0.05) | 10 | 0.589 |
| 290–390 (Mn = 0.05) | 10 | 0.443 |
| 400–500 (Mn = 0.05) | 10 | 0.204 |
| 180–280 (Fe = 0.05) | 10 | 0.424 |
| 290–390 (Fe = 0.05) | 10 | 0.393 |
| 400–500 (Fe = 0.05) | 10 | 0.168 |

*R3c* space group with rhombohedral symmetry. Microstructural analysis of the surface of the compounds by scanning electron microscopy (SEM) exhibits that there is a significant change in grain size. All the samples exhibit ferroelectric to paraelectric transition. The decrease of activation energy and the increase of AC conductivity have been observed for the Mn/Fe-doped sample which may be due to the decrease of lattice parameters, cell volume, and bond lengths with the increase in Mn/Fe concentration. The activation energy is found to be maximum at ferroelectric region and minimum at paraelectric region for both the samples (Mn and Fe). It is observed that the activation energy is less for Mn-doped sample compared to that of Fe-doped sample which leads to higher conductivity for Mn-doped sample. The maximum barrier height ($W_m$) is found to be 3.34 eV, and it is confirmed that the conduction mechanism is bipolaron type for Mn (5%) doped sample.

## Conflict of Interests

This research is the authors' original work. They do not have a direct or indirect financial relation with any commercial identity mentioned in this paper. This paper is of the authors' only and they all agreed on its publication.

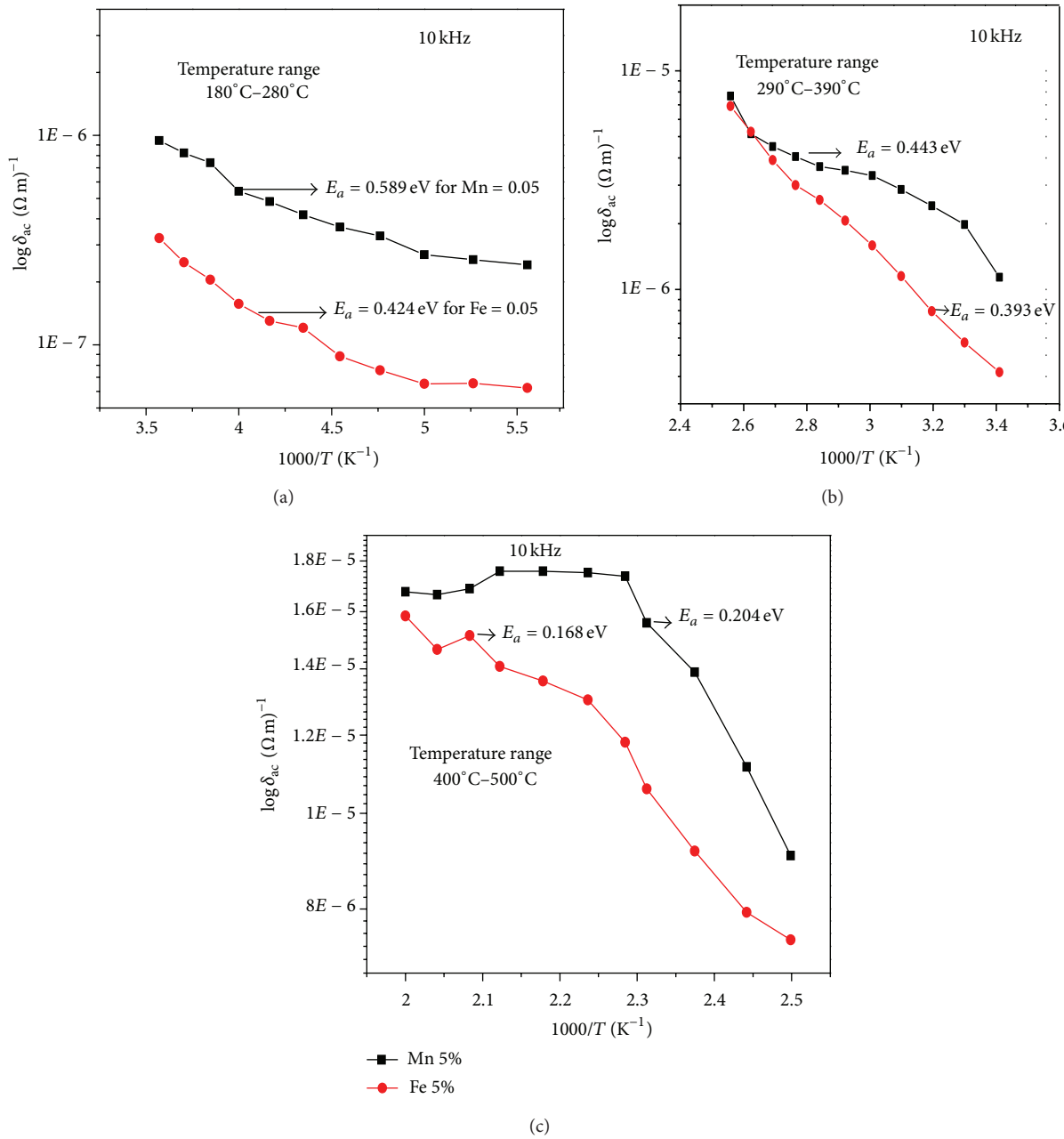


FIGURE 10: (a–c) Variation of log $\delta_{ac}$ conductivity versus inverse of temperature of the samples $Pb(Zr_{0.60}Mn_{0.05}Ti_{0.35})O_3$ and $Pb(Zr_{0.60}Fe_{0.05}Ti_{0.35})O_3$ at frequency 10 kHz with error bar being plus or minus 0.05%.

## Acknowledgments

The authors are grateful to Dr. A. K. Thakur, Department of Physics and Meteorology, Indian Institute of Technology, Kharagpur, India, for his useful suggestions and for offering his laboratory for dielectric measurements.

## References

[1] M. E. Lines and A. M. Glass, *Principles and Applications of Ferroelectrics and Related Materials*, Oxford University Press, Oxford, UK, 1977.

[2] G. Shirane and S. Hoshino, "On the phase transition in lead titanate," *Journal of the Physical Society of Japan*, vol. 6, pp. 265–270, 1951.

[3] H. P. Klung and L. B. Alexander, *X-Ray Diffraction Procedures*, John Wiley & Sons, New York, NY, USA, 1974.

[4] B. Jaffe, W. R. Crook, and H. Jaffe, *Piezoelectric Ceramics*, Academic Press, New York, NY, USA, 1971.

[5] L. Radhapiyari, A. R. James, O. P. Thakur, and C. Prakash, "Structural and dielectric properties of Fe-substituted BST thin films grown by laser ablation," *Materials Science and Engineering B*, vol. 117, pp. 5–9, 2005.

[6] P. Novak, J. Kunes, L. Chaput, and W. E. Pickett, "Exact exchange for correlated electrons," *Physica Status Solidi B*, vol. 243, pp. 563–572, 2006.

[7] H. Yokota, N. Zhang, A. E. Taylor, P. A. Thomas, and A. M. Glazer, "Crystal structure of the rhombohedral phase of $PbZr_{1-x}TixO_3$ ceramics at room temperature," *Physical Review B*, vol. 80, Article ID 104109, 12 pages, 2009.

[8] S. Singh, O. P. Thakur, D. S. Rawal, C. Prakash, and K. K. Raina, "Improved properties of Sm substituted PCT ceramics using microwave sintering," *Materials Letters*, vol. 59, no. 7, pp. 768–772, 2005.

[9] G. H. Heartling, "Ferroelectric ceramics: history and technology," *Journal of the American Ceramic Society*, vol. 82, pp. 797–818, 1999.

[10] N. Sahu, M. Kar, and S. Panigrahi, "Rietveld refinement of a nanocrystalline $Pb_{0.5}Z_{0.5}TiO_3$ Ceramics," *International Journal of Physics*, vol. 3, pp. 157–164, 2010.

[11] T. Ohno, D. Suzuki, K. Ishikawa, and H. Suzuki, "Size effect for lead zirconate titanate nano-particles with PZT(40/60) composition," *Advanced Powder Technology*, vol. 18, no. 5, pp. 579–589, 2007.

[12] B. Tiwari and R. N. P. Choudhary, "Frequency-temperature response of $Pb(Zr_{0.65-x}Ce_xTi_{0.35})O_3$ ferroelectric ceramics: structural and dielectric studies," *Physica B*, vol. 404, no. 21, pp. 4111–4116, 2009.

[13] N. Sahu, S. Panigrahi, and M. Kar, "Structural investigation and dielectric properties of Mn Substituted $Pb(Zr_{0.65}Ti_{0.35})O_3$ Perovskite," *Ceramics International*, vol. 38, no. 2, pp. 1549–1556, 2012.

[14] S. Sen, P. Pramanik, and R. N. P. Choudhary, "Effect of Ca-additions on structural and electrical properties of $Pb(SnTi)O_3$ nano-ceramics," *Ceramics International*, vol. 33, no. 4, pp. 579–587, 2007.

[15] N. Sahu, S. Panigrahi, and M. Kar, "Structural study of Zr doped $PbTiO_3$ materials by employing Rietveld method," *Advanced Powder Technology*, vol. 22, pp. 689–694, 2011.

[16] Ragini, A. K. Singh, R. Ranjan, and D. Pandey, "Monoclinic Phase in the $Pb(Zr_xTi_{1-x})O_3$ ceramics," *Pandey Ferroelectrics*, vol. 35, p. 325, 2005.

[17] N. Sahu, M. Kar, S. Panigrahi, and R. Refinement, "Microstructure and electrical properties of $PbTiO_3$ ceramic materials," *Archives of Physics Research*, vol. 1, pp. 75–87, 2010.

[18] Ragini, R. Ranjan, S. K. Mishra, and D. Pandey, "Room temperature structure of $Pb(Zr_xTi_{1-x})O_3$ around the morphotropic phase boundary region: a rietveld study," *Journal of Applied Physics*, vol. 92, no. 6, article 3266, 9 pages, 2002.

[19] T. Takahashi, "Lead titanate ceramics with large piezoelectric anisotropy and their applications," *American Ceramic Society Bulletin*, vol. 69, pp. 691–695, 1990.

[20] C. Tanasoiu, E. Dimitriu, and C. Miclea, "Effect of Nb, Li doping on structure and piezoelectric properties of PZT type ceramics," *Journal of the European Ceramic Society*, vol. 19, no. 6-7, pp. 1187–1190, 1999.

[21] N. Sahu and S. Panigrahi, "Rietveld analysis of $La^{3+}/Al^{3+}$ modified $PbTiO_3$ ceramics," *Ceramics International*, vol. 38, no. 2, pp. 1085–1092, 2012.

[22] B. M. Jin, J. Kim, and S. C. Kim, "Effects of grain size on the electrical properties of $PbZr_{0.52}Ti_{0.48}O_3$ ceramics," *Applied Physics A*, vol. 65, no. 1, pp. 53–56, 1997.

[23] A. Ghosh, "Ac conduction in iron bismuthate glassy semiconductors," *Physical Review B*, vol. 42, no. 2, pp. 1388–1393, 1990.

[24] K. Shimakawa and T. Itoh, "Grain boundary scattering of free electrons in Ga-doped microcrystalline zinc oxide films," *Japanese Journal of Applied Physics*, vol. 46, no. 20–24, pp. L577–L579, 2007.

[25] R. A. Young, *The Rietveld Method*, International Union of Crystallography, Oxford University Press, New York, NY, USA, 1996.

[26] A. Taylor, *X-Ray Metallography*, John Wiley & Sons, New York, NY, USA, 1961.

[27] O. P. Thakur, C. Prakash, and A. R. James, "Enhanced dielectric properties inmodified barium titanate ceramics through improved processing," *Journal of Alloys and Compounds*, vol. 470, no. 1-2, pp. 548–551, 2009.

[28] C. Prakash, O. P. Thakur, and P. Kishan, "Improvement in material figure of merit of PLZT by samarium substitution," *Ferroelectrics*, vol. 263, no. 1, pp. 61–66, 2001.

[29] B. Tiwari and R. N. P. Choudhary, "Effect of Mn-substitution on structural and dielectric properties of $Pb(Zr_{0.65-x}Mn_xTi_{0.35})O_3$ ceramics," *Solid State Sciences*, vol. 11, no. 1, pp. 219–223, 2009.

[30] J. M. Herbert, *Ferroelectric Transducers and Sensors*, Gordon and Breach Science Publishers, London, UK, 1985.

[31] A. K. Jonscher, "The "universal" dielectric response," *Nature*, vol. 267, no. 5613, pp. 673–679, 1977.

[32] X. Dai, Z. Xu, and D. Viehland, "Effect of oxygen octahedron rotations on the phase stability, transformational characteristics, and polarization behavior in the lead zirconate titanate crystalline solution series," *Journal of the American Ceramic Society*, vol. 78, no. 10, pp. 2815–2827, 1995.

[33] S. R. Elliott, *Physics of Amorphous Materials*, Longmans, London, UK, 2nd edition, 1990.

[34] K. H. Härdtl and D. Hennings, "Distribution of A-site and B-site vacancies in (Pb, La)(Ti, Zr)$O_3$ ceramics," *Journal of the American Ceramic Society*, vol. 55, pp. 230–223, 1972.

[35] A. Majchrowski, E. Michalski, J. Zmija, L. R. Jaroszewicz, and I. V. Kityk, "Temperature anomalies of the laser stimulated elastooptical effect in $PbZrO_3$ single crystals," *Materials Letters*, vol. 84, pp. 114–115, 2012.